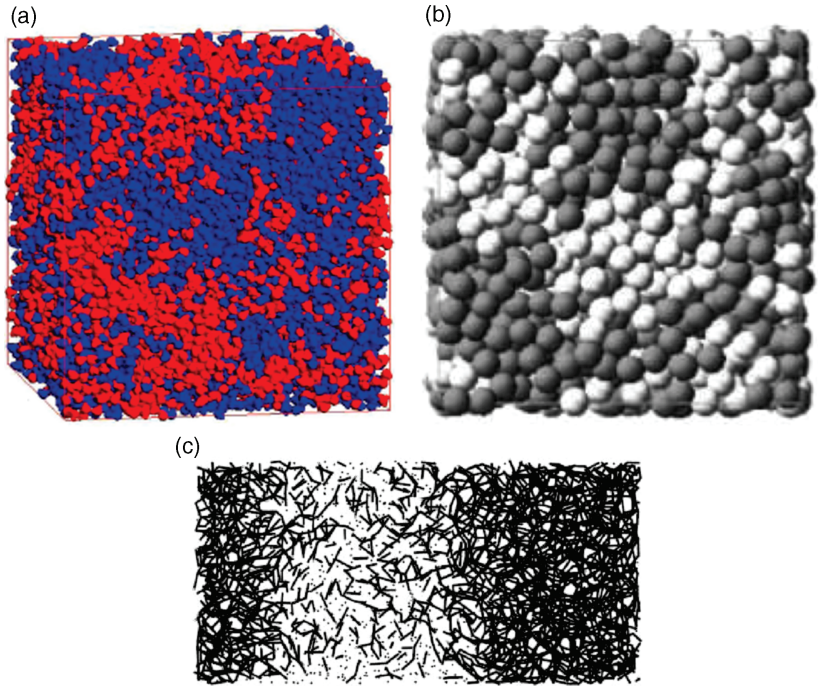

Figure 6.2. Snapshots from computer simulations showing the coexistence between LDL and HDL in different polymorphic liquids. (**a**) Water. Dark and light molecules belong to LDL and HDL, respectively. (**b**) Silica. Dark and light spheres represent Si atoms in the HDL and LDL phase, respectively. For clarity, O atoms are not shown. (**c**) System of particles interacting via the isotropic Jagla potential (see Fig. 8). LDL and HDL particles are both represented by dots. Lines connect pairs of particle belonging to HDL. (a), (b), and (c) are taken from Refs [33], [35], and [36], respectively.

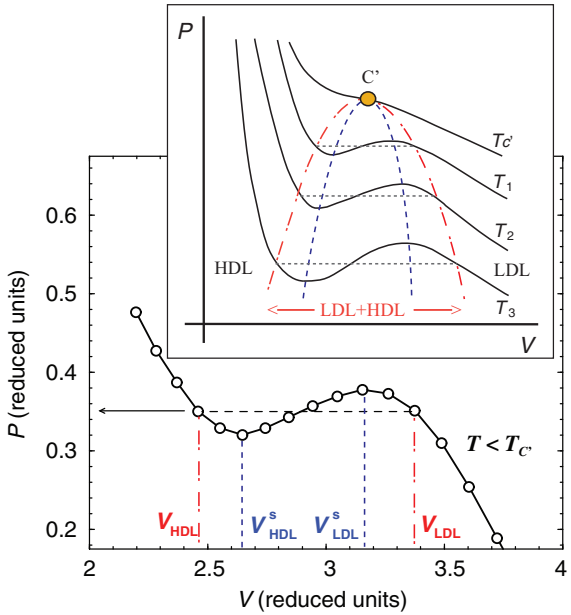

Figure 6.3. Pressure versus volume isotherm at $T < T_{C'}$ obtained from simulations of a system of particles interacting via the Fermi-Jagla pair potential, a smooth version of the Jagla pair potential shown in Fig. 8a [38]. The loop in $P(V)$ occurs for volumes in which LDL coexist with HDL. In this volume range, the equilibrium isotherm is given by the horizontal dashed line that is obtained using the Maxwell construction [37]. LDL is stable at $V \geq V_{\rm LDL}$ and metastable, relative to HDL, at $V^{\rm s}_{\rm LDL} < V < V_{\rm LDL}$. Similarly, HDL is stable at $V \leq V_{\rm HDL}$ and metastable, relative to LDL, at $V^{\rm s}_{\rm HDL} > V > V_{\rm HDL}$. The minima and maxima of the $P(V)$ isotherms define the HDL and LDL spinodal lines, respectively, and are shown schematically in the inset (blue curves). Red lines in inset indicate the limits of stability of LDL and HDL. C' is the LLCP; $T_3 < T_2 < T_1 < T_{C'}$.

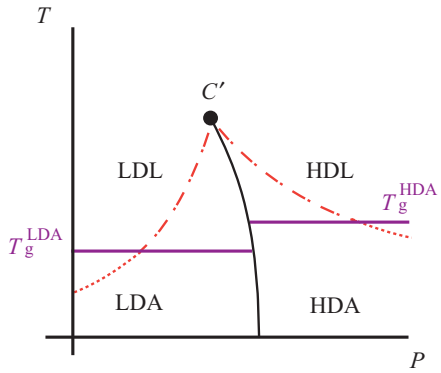

Figure 6.4. Schematic phase diagram of polymorphic liquid showing the LL first-order phase transition line ending at the LLCP, C'. The right and left dash-dotted curves are the LDL and HDL spinodal lines, respectively. T_g^{LDA} and T_g^{HDA} are the glass transition temperatures of LDA and HDA, respectively, and may depend on pressure. Fast cooling of LDL and HDL below the corresponding glass transition temperature results in LDA and HDA, respectively.

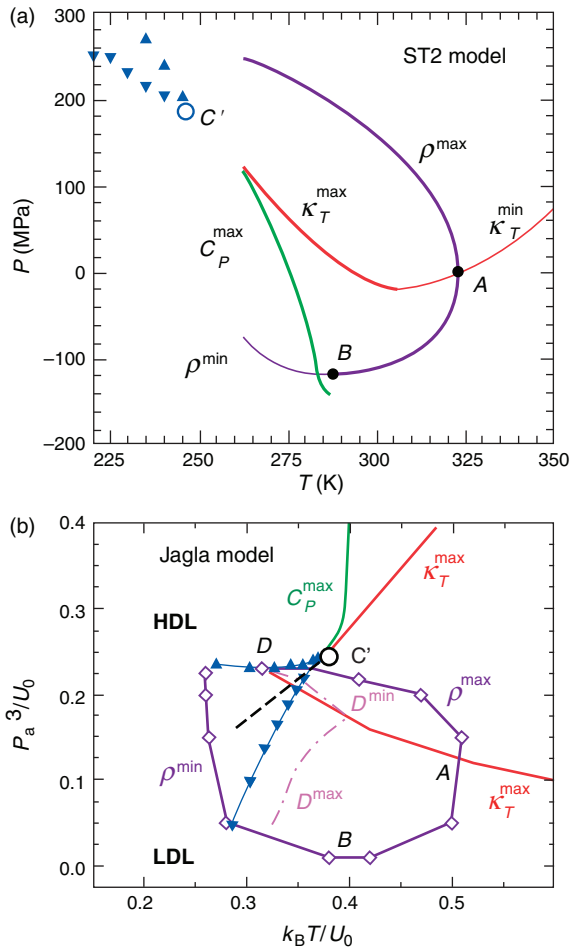

Figure 6.5. Maxima and minima lines in the supercritical region of the (a) ST2 water and (b) Jagla models. κ_T^{max}, C_P^{max}, and ρ^{max} are the maximum compressibility, specific heat, and density lines; κ_T^{min} and ρ^{min} are the minimum compressibility and density lines. Up and down triangles indicate the LDL and HDL spinodal lines, respectively; both lines end at the LLCP, C'. Points A and B are extrema of the ρ^{max} line. The ρ^{max} line reaches a minimum pressure at point B, at which the ρ^{max} and ρ^{min} lines merge. The ρ^{max} line reaches a maximum temperature at point A, at which the ρ^{max} and extrema compressibility line (κ_T^{max} or κ_T^{min} line) intersect one another. Point D in (b) is the minimum of the LDL spinodal line at which the ρ^{max} line terminates. Included in (b) are the maximum and minimum diffusivity lines, D^{max} and D^{min} lines, respectively (magenta dash-dotted line). (a) and (b) are adapted from Refs [43] and [44], respectively.

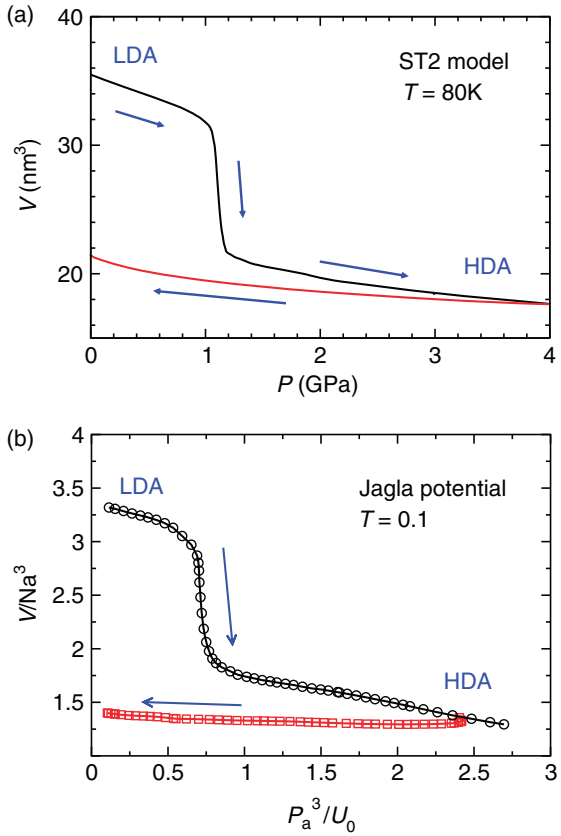

Figure 6.7. Pressure dependence of the volume during the LDA-to-HDA transformation and subsequent decompression of HDA. Results are obtained from computer simulations of (**a**) water, using the ST2 model, and (**b**) a system of particles interacting via the Jagla potential (defined in Fig. 8a). At the simulated temperatures, the LDA-to-HDA transformation is not reversible. (a) and (b) are remarkable similar to the experimental results shown in Fig. 6a. (a) and (b) are adapted from Refs. [67] and [63], respectively.

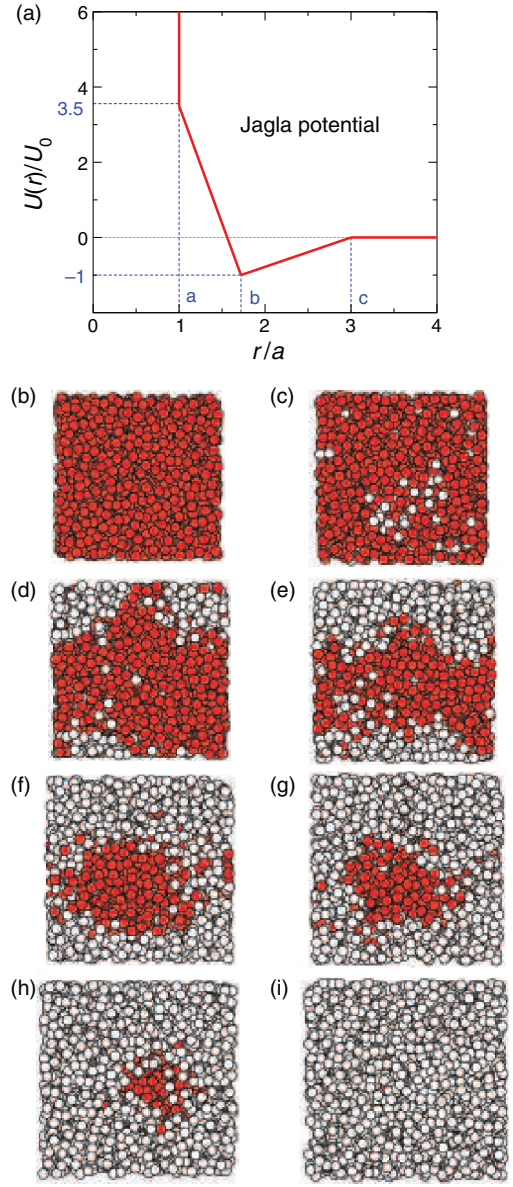

Figure 6.8. (**a**) The spherically symmetric two-scale Jagla potential with attractive and repulsive ramps. Here a is the hard-core diameter, $b = 1.72a$ is the soft-core diameter, and $c = 3a$ is the long distance cutoff. U_0 is the minimum energy. (**b**)–(i) Snapshots of a system of particles interacting via the Jagla potential during the HDA-to-LDA decompression at $T = 0.15$. Snapshots are taken at different times as HDA (red spheres) transforms into LDA (white spheres). LDA is composed of particles with fewer than two neighbors within a distance $r_c = 1.3a$. Phase separation is observed between HDA and LDA, indicating that LDA and HDA are indeed separated by a sharp first-order-like (amorphous-to-amorphous) phase transition. Figures taken from Ref. [63].

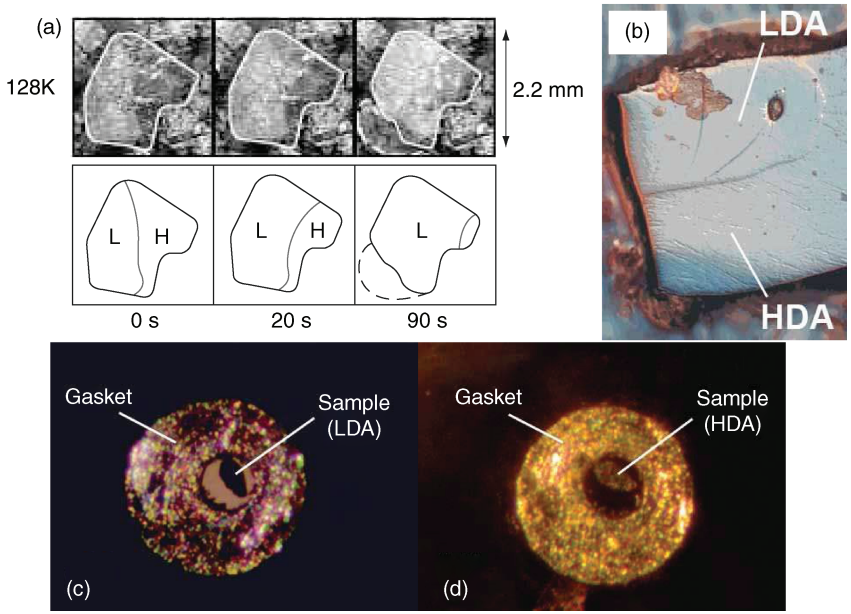

Figure 6.9. Photographs from experiments showing coexistence between LDA and HDA. (**a**) Visual observation of the LDA-to-HDA transformation in amorphous water upon annealing LDA at $T = 128$K and $P = 1$ atm. The transformation proceeds from left to right. The location and width of the LDA-HDA boundary region are shown schematically in the bottom panels (L = LDA; H = HDA). The broken line shows the ice separated by a crack. From Ref. [71]. (**b**) Y_2O_3-–Al_2O_3 glassy sample containing ≈ 20 mol% of Y_2O_3, formed by quenching the liquid. The sample in the picture was polished. Since LDA and HDA have different mechanical properties (but same composition), polishing allows to distinguish the LDA and HDA domains. LDA is mechanically more resistant, has higher relief than HDA, and an absence of polishing scratches [72]. (c) and (d) Optical micrograph of an amorphous Si sample using a combination of reflected and transmitted light for illumination. The LDA sample is black and nonreflective, compared to the surrounding metal gasket. Instead, the HDA sample appears highly reflective and is similar in appearance to the metal gasket. From Ref. [61].